Large Area Self-Assembly of Nematic Liquid-Crystal-Functionalized Gold Nanorods

*S. Umadevi, Xiang Feng, and Torsten Hegmann**

Fascinating nematic- and smectic-like self-assembled arrays are observed for gold nanorods partially capped with either laterally or terminally attached nematic liquid crystals upon slow evaporation of an organic solvent on TEM grids. These arrays can be manipulated and reoriented by applying an external magnetic field from quasi-planar to vertical similar to a Fréedericksz transition of common organic nematic liquid crystals. Birefringence and thin film textures of these self-assembled gold nanorod arrays observed by polarized optical microscopy are strongly reminiscent of common organic nematic liquid crystal textures between crossed polarizers and, additionally, support the formation of ordered liquid crystal-like anisotropic superstructures. The ordering within these arrays is also confirmed in bulk samples using small angle X-ray scattering (SAXS).

1. Introduction

In the last few years, anisotropic metal nanostructures attract a great deal of interest compared to their spherical counterparts owing to their unique shape dependent properties such as multiple plasmon bands, light absorption in the near infrared, enhanced electromagnetic fields at nanorod tips among others, promising various potential applications in optics and photonics.[1–7] Gold nanorods (GNRs), in particular have gained significant interest due to their proven applications in sensing,[2–5] cellular imaging[3,8] and cancer therapy.[9] Obtaining ordered assemblies of GNRs over an extended area is an active research topic in nanoscience since the resulting enhanced collective properties of such assemblies differ from the properties of their individual components. Organized GNR assemblies have attractive applications in surface-enhanced Raman spectroscopy and fluorescence sensing.[10] Although great advances have been made regarding the self-assembly of spherical metal nanoparticles, obtaining organized arrays of anisotropic nanorods with a tunable shape and size is still a challenging task because their assembly requires both orientational and positional ordering. Several strategies have been pursued to organize anisotropic nanorods into ordered superstructures.[4–6] Nikoobakth et al. reported superlattices of GNRs by employing a mixture of the surfactants hexadecyltrimethylammonium bromide (HTAB) and tetraoctylammonium bromide (TOAB) as capping ligands.[11] The Langmuir-Blodgett technique was used by Kim and coworkers to demonstrate a pressure induced isotropic-nematic-smectic transitions of inorganic nanorods.[12] Solvent evaporation on TEM grid was shown to result in the assembly of CTAB stabilized GNRs by Sau and Murphy.[13] Sreeprasad et al. utilized the charge neutralization of CTAB-capped GNRs by dimercaptosuccinic acid and EDTA, ultimately leading to the formation of one-, two-, and three-dimensional superstructures of GNRs.[14] Two- and three-dimensional arrays of hydrophobic GNRs by solvent evaporation on a substrate were also reported by Mitamura and co-workers.[15] One of the first examples using soft-matter templates was the self-assembly of GNRs into 1D and 2D structures using DNA as template.[16] More recently, three-dimensional superstructures of (1-mercaptoundec-11-yl)-hexa(ethylene glycol)-capped GNRs having a local smectic B order have been described by Hamon et al.[17] They employed a novel drying method in which GNRs crystallization was carried out between smooth surfaces and a topographically patterned stamp.

In many of these above-mentioned systems, the assembly formation is carried out in aqueous medium and further manipulation of the formed assembly is quite difficult or impossible. Therefore, a versatile method for the large scale organization of GNRs allowing for simultaneous formation and control over the morphology of the final self-assembled superstructure would be a great advantage for technological application of these materials.

Herein, we describe a novel strategy to assemble GNRs into ordered superstructures by chemically functionalizing GNRs with an aspect ratio of about four with thermotropic nematic liquid crystals (LCs) simultaneously acting as stabilizing ligand as well as tunable template. Nematic LCs are one-dimensionally ordered fluids whose anisotropic structures gives rise to unique orientational, optical and electro-optical properties that can be easily controlled by external stimuli such as electric or magnetic fields. By associating LCs with nanoparticles it is possible to impart order and fluidity to nanosystems. More importantly,

Dr. S. Umadevi,[+] X. Feng, Prof. T. Hegmann
Department of Chemistry
University of Manitoba
Winnipeg, MB, R3T 2N2, Canada
Prof. T. Hegmann
Chemical Physics Interdisciplinary Program
Liquid Crystal Institute
Kent State University
Kent, OH 44242, USA
E-mail: thegmann@kent.edu
[+]Present address: Central Electrochemical Research Institute, Karaikudi-630 006, Tamilnadu, India

DOI: 10.1002/adfm.201202727

however, the final self-assembled LC-hybrid nanostructure can be manipulated by external stimuli to bring about morphological changes. All three major type of thermotropic LCs namely the rod-,[18–25] disc-[26,27] and bent-core[28] LCs have been covalently attached to gold nanoparticles (GNPs) and these systems were found to exhibit remarkable self-assembly behavior either on a substrate or in the bulk. LCs have also proven to be promising candidates to assemble GNRs. Park et al.[29] described the self-organization of GNRs either in side-by-side or end-to-end fashion using self-assembled stacks of lyotropic chromonic LC materials. Liu and co-workers[30] demonstrated the bulk alignment of GNRs dispersed in surfactant-based lyotropic LCs and their realignment by shearing or application of a magnetic field. Very recently, we have reported the magnetic field induced formation of self-assembled arrays of nematic LC functionalized GNRs with the mesogens attached to the nanorod surface at one of the terminal hydrocarbon chains via a siloxane linkage (**LC1**), i.e., mesogens and GNR long axes are in theory perpendicular to one another (**Figure 1**a).[31] The silane conjugation approach provides access to thermally and chemically robust GNRs that do not aggregate in solution due to the small quantity of trapped surfactant (CTAB) allowing for sufficient electrostatic repulsion between the GNRs. In this particular case, the mesogens attached to the GNR surface align with the external magnetic field producing a planar array of the GNRs on the transmission electron microscopy (TEM) grid as shown in the TEM image and cartoon in Figure 1a. These examples clearly highlight the significance of LC molecules for the creation and manipulation of anisotropic nanostructures.

To further explore the role of the relative mesogen connectivity to the GNR surface and its impact on GNR self-organization, we synthesized GNRs where the thermotropic nematic mesogens are attached to the GNR surface via a lateral alkyl chain in a side-on rather than an end-on fashion (idealized, mesogen and GNR long axis are parallel), and studied their self-assembly upon slow solvent evaporation on substrates (Figure 1b). The preference for this particular ligand type to functionalize GNRs emerges from the fact that laterally substituted LC ligands show the tendency to induce nematic ordering when linked to large molecules such as polymers, dendrimers and even to quasi-spherical (polyhedral) gold nanoparticles (NPs) as shown by Cseh et al.[20] Extensive studies on the mesophase exhibited by these gold NPs revealed highly ordered rhombohedral or hexagonal columnar arrangements of the particles themselves.[22] In order to explain these experimental observations the authors proposed that in the mesophase the NPs are arranged in columns surrounded by a nematic sheath and that these columns spontaneously self-organize yielding complex periodic lattices. Such spatial arrangement would be an ideal platform for creating ordered superlattices of GNRs, by factually replacing the NP columns in Cseh's work with individual LC-capped GNRs (Figure 1b).

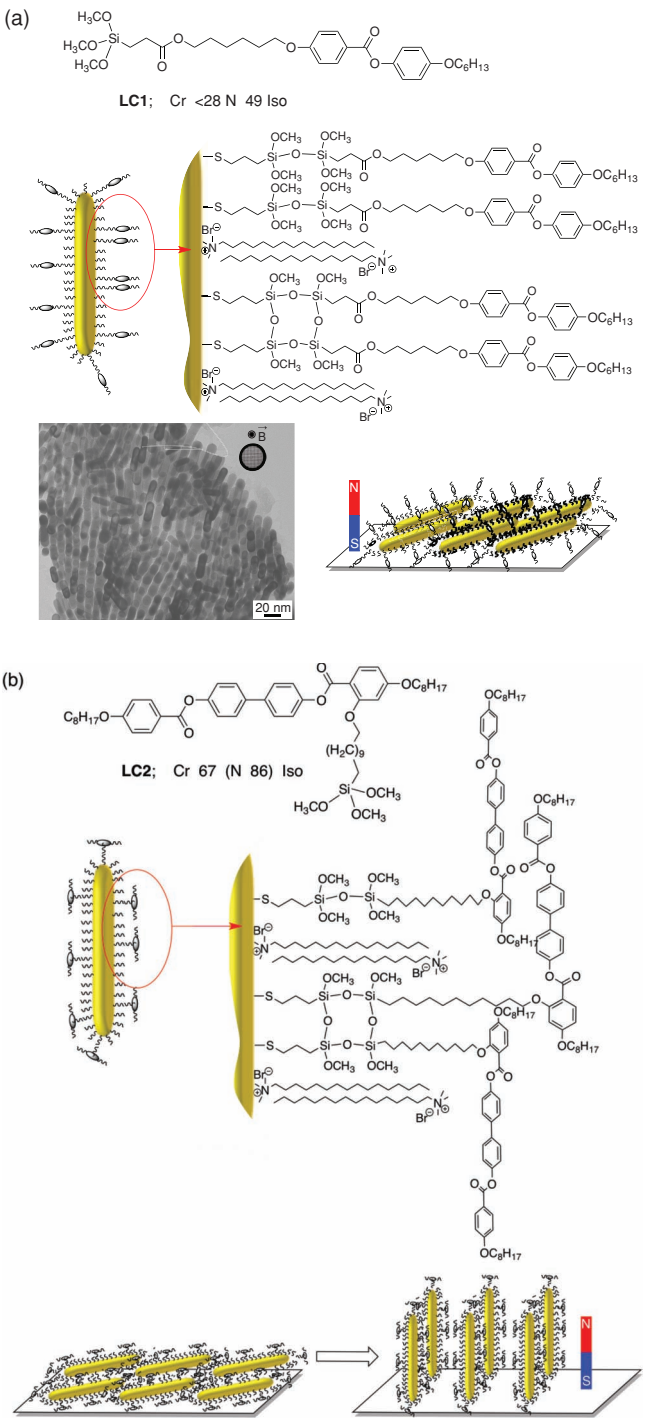

Figure 1. Schematic representation of nematic LC-functionalized GNRs and their observed or expected self-assembly upon slow evaporation of the solvent: a) end-on mesogen attachment. The inset in the TEM image shows the orientation of the magnetic field with respect to the TEM grid[31] and b) Side-on mesogen attachment with the proposed Fréedericksz-type transition of the LC-functionalized GNRs.

2. Results and Discussion

The precursor nematic LC (**1**) of the rod-shaped nematic siloxane **LC2** features two octyloxy chains at the two terminal ends of the rod-like molecules and a vinyl-terminated lateral hydrocarbon chain. Compound **1** was prepared following a procedure previously reported in the literature.[32] The compound exhibits a nematic phase with the following phase transition

temperatures (°C): Cr 91 N 146 Iso on heating (reported transition temperatures (°C): Cr 93 N 141 Iso[33]) and crystallizes well below room temperature on cooling. The terminal alkene of mesogen **1** was converted to a trimethoxysilane end group by a hydrosilylation reaction as shown in **Figure 2**a. The procedure followed to prepare silane **LC2** from **1** along with its analytical data are provided in the experimental section. POM observation of this silane showed a monotropic nematic phase with the following transition temperatures (°C): Cr 67 (N 86) Iso.[#]

The precursor CTAB stabilized GNRs were prepared at 30 °C by a single step, non-seeding method.[31,34] The rods were characterized by UV-vis-NIR and TEM. The UV-vis-NIR spectrum of these GNRs showed two absorption maxima, situated at 512 nm and 759 nm corresponding to the transverse surface plasma resonance (TSPR) and the longitudinal surface plasma resonance (LSPR), respectively (Figure 2c). The relative narrow width of the LSPR indicated the monodispersity of the formed nanorods, which was further confirmed by TEM imaging (Figure 2b), and the low degree of aggregation. It can be seen from the TEM image that the percentage of the unwanted spherical particles is comparatively low. The length and diameter of the rods are 28.6 ± 2 nm and 6.5 ± 1.5 nm, respectively,

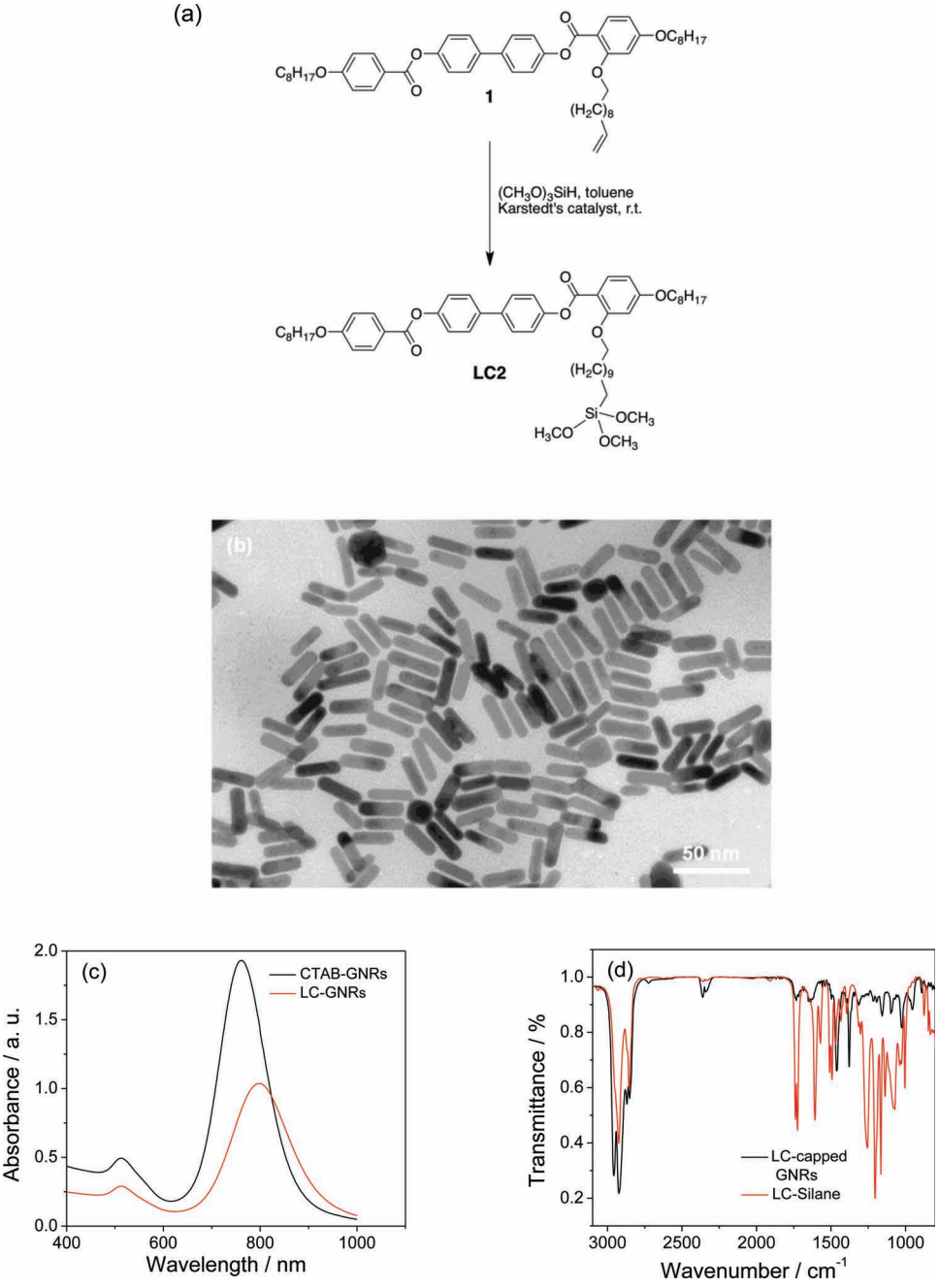

Figure 2. a) Synthesis of the LC silane **LC2**. b) TEM image obtained for CTAB stabilized GNRs in water. c) UV-vis-NIR spectra recorded for the CTAB-capped GNRs and **LC2**-capped GNRs. d) Overlapped IR spectra of the **LC2**-capped GNRs and LC-silane.

leading to an aspect ratio of ≈4.3, as determined by TEM. Also, it is apparent from the image that the rods show only short-range side-by-side assembly with no in-plane correlation.

The exchange of the CTAB capping on the GNRs with the nematic silane **2** was carried out in a two-step silane condensation reaction as described by us recently.[31] In the first step, some of the CTAB ligands on the nanorod surface were replaced by a mercaptotrimethoxy silane (MPS), which binds to the GNR surface through a strong Au-S covalent linkage. In the second step, the nematic silane was added followed by base to bring about the hydrolysis of trimethoxy silane groups and subsequent condensation among the silanols to provide a stable, partial or patchy oligo(siloxane) network around the GNRs. The phase transfer of GNRs from aqueous to organic phase upon ligand exchange can be visually observed as a change in color of the aqueous and organic phases (see Supporting Information, Figure S1).

The capping exchange from CTAB to LC silane was confirmed by both UV-vis-NIR spectrophotometry and IR spectroscopy. After the exchange process, the maximum of LSPR band red-shifted from 759 nm to 798 nm (Figure 2c), which is an indication of the change in the dielectric environment surrounding the GNRs. The maximum wavelength, λ_{max}, of the LSPR is particularly sensitive to changes in the surrounding dielectric (i.e., changes of the refractive index of the surrounding medium due to the nature of the coating; a CTAB vs. LC silane exchange leads an increase in the dielectric constant of the surrounding medium).[35] A red shift of the LSPR of around 30 nm is commonly observed for replacements of CTAB with other capping agents.[35,36] Further, IR provided clear evidence for the presence of the LC ligand on the nanorod surface. The IR spectrum obtained for the well-washed sample of LC-capped GNRs (no excess free LC silane) displayed all the bands characteristic of the LC-silane along with a Si-O-Si stretching vibration corresponding to siloxane bonds (Figure 2d). Overlapping the IR spectra of the LC-coated GNRs with that of the LC-silane clearly illustrates that the IR pattern of the former follows that of the latter with only one exception, the bands are slightly shifted to lower wavenumbers. The sharp bands at 2957, 2918, 2859, 1457, and 1378 cm^{-1} correspond to the antisymmetric stretching of CH_3 groups, antisymmetric stretching and symmetric stretching of CH_2 groups, bending mode of CH_2 groups and rocking vibrations of CH_3 groups, respectively. More importantly, the spectrum shows stretching bands at 1733 and 1158 cm^{-1} (and 1023 cm^{-1}) corresponding to ester –C=O and –C-O stretching modes. Further, the spectrum shows bands in the region 1000–1100 cm^{-1} (1096, 1025 and 953) that are due to the Si-O-Si stretching mode of the siloxane bond (1096 and 1025 cm^{-1}) and the Si-O-C stretching mode of trialkoxysilane groups (1090 and 953 cm^{-1}). Incidentally, corresponding peaks at almost matching wavenumbers have been reported for other silane condensations on GNRs[31] and other substrates (1090 cm^{-1} and 1033 cm^{-1}).[37] As seen from the spectrum, some of the bands recorded for functionalized GNRs are broad as expected for such hybrid nanomaterials. The occurrence the Si-O-C stretching band in the GNR hybrid spectrum suggests the presence of non-hydrolyzed trimethoxy groups of the silane. However, the ^1H NMR spectrum of the supernatant obtained right after the coating exchange clearly indicated that overall at least one methoxy group of the silane was hydrolyzed and hence available for condensation. This analysis was performed by integrating the area under the peak at 3.6 ppm corresponding to the methoxy groups linked to the Si (see Supporting Information, Figure S2). The spectrum also showed that the ester linkages in the silane remain intact under the basic condition used for the silane condensation. Hence, only a partial or "patchy siloxane network" is formed during the two-step GNR surface modification step, which nonetheless produced GNRs that are thermally, chemically and colloidal stable over extended time periods.

To investigate if decorating GNRs with nematic LCs via lateral hydrocarbon spacers produces well-organized superstructures with one- or two-dimensionally ordered nematic and smectic-like morphologies we performed detailed, extensive TEM and high-resolution TEM studies.

A 2–3 μL drop of the colloidal solution of the once-washed GNR sample (taken from a 1 mL GNR dispersion containing ≈150 μL of 10 mM free ligand; i.e., about 5 wt% free vs 95 wt% bound to the GNR surface) in toluene was drop-casted on carbon-coated copper grids and allowed to dry under ambient conditions. Among the various solvent systems and solution concentrations examined for the self-assembly process, a highly concentrated sample (absorbance of the nanorod dispersion at 798 nm was ≈3.5 in a 1 cm path length cuvette) in toluene was found to give remarkable results. The observation of such a sample using TEM revealed highly ordered 3D superstructures of GNRs in almost every part of all grids investigated. In addition, assemblies with different morphologies were seen in different regions of the same grid for any given sample. This might be due to the high concentration of the sample causing the thin solvent film to break into unsymmetrical regions over the grid before the solvent evaporation takes place, ultimately resulting in different local GNR concentrations.[13,38] **Figure 3** shows representative TEM images of the densely packed, highly organized 3D patterns of the **LC2**-coated GNRs. It can be seen from Figure 3a,b that the rods assume a staggered arrangement near the ends of the assembly; however they gradually translate to form an end-to-end, eclipsed chain-like pattern in the vicinity of the center. Further, it is interesting to point out here that these chains are spaced evenly next to each other. In this assembly, some of the rods appear to be shorter (for example, those circled in red) than their original size (rods circled in yellow), likely because these rods are oriented at an angle (between 0 and 90°) to the substrate and not perfectly parallel to the substrate. Very few axially oriented (at a 90° angle) rods can also be seen at the top left corner (green circle) of the Figure 3a. Similar end-to-end attached parallel wavy structures of the rods in two different regions of the same grid, extending over several hundred nanometers are shown in Figure 3b,c. Another fascinating well-oriented multilayer 3D smectic-like pattern is shown in Figure 3d. The dark region towards the right side of the figure indicates the increased thickness of the assembly.

In other areas of the TEM grid, unique superstructures were observed in which smectic arrays of GNRs were self-assembled in two different fashions, situated next to each other as shown in **Figure 4**a. In the left region of Figure 4a the GNRs form parallel packed end-to-end connected chains extending over several hundred nanometers. The thickness of the assembly increases from top to bottom as indicated by the increased darkness at

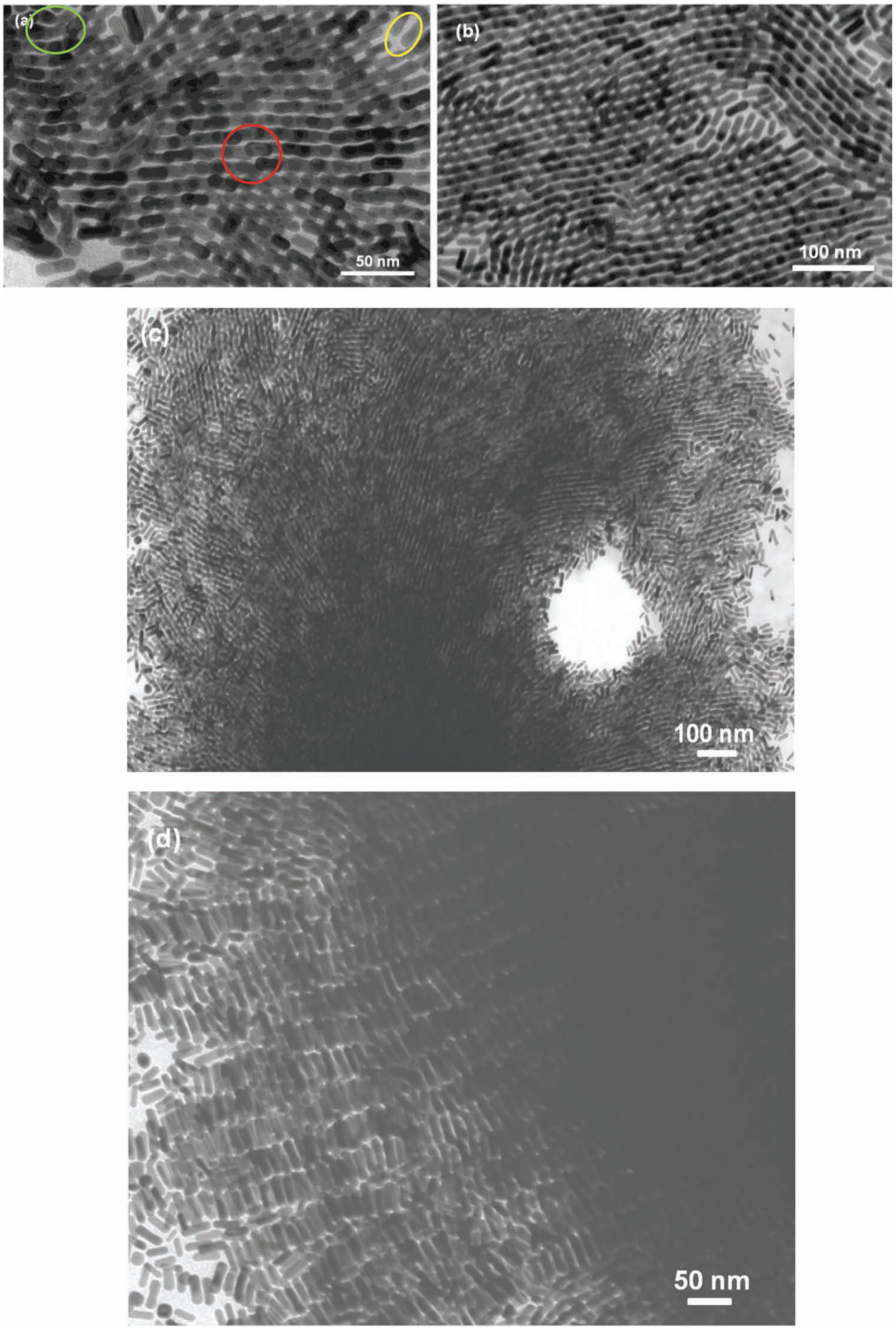

Figure 3. a–c) TEM images showing the highly organized assemblies of **LC2**-functionalized GNRs in different regions of the same grid. d) A 3D smectic array of the GNRs.

the bottom regions of the image. The end-to-end eclipsed arrangement of the nanorods is so precise that these chains appear as perfectly uniform lines, making it very difficult to even visually isolate individual nanorods. Further, one can also see the regularity in the inter-chain distances. The right half of the figure displays a 3D smectic-like structure generated by a parallel orientation of the rods with respect to one another. In particular, this highly ordered structure consists of several layers of side-by-side arranged rods forming 3D assemblies (see multilayer pattern in the right top area of Figure 4a).

More interestingly, in some parts of the grid, assemblies extending over several sq μm^2 were observed. One such

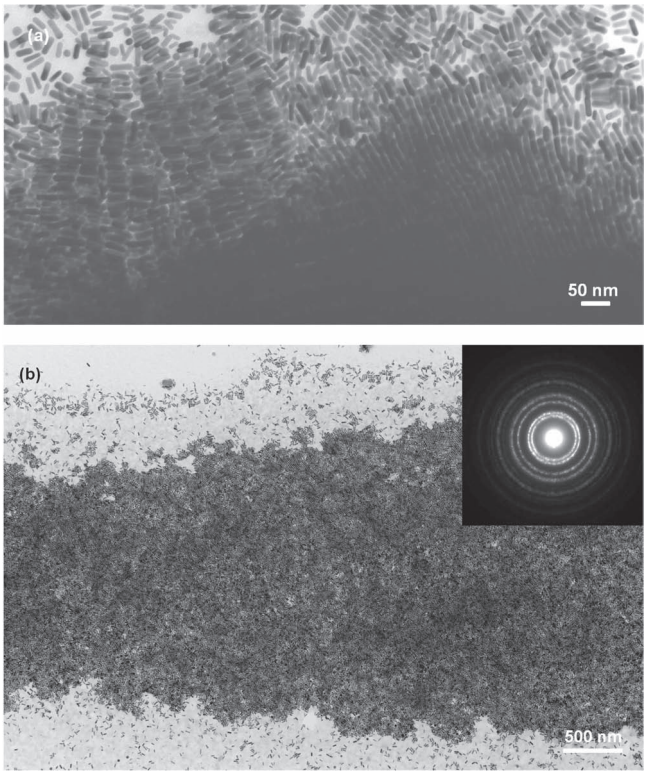

Figure 4. a) TEM image showing the smectic arrays of LC-capped GNRs arranged in two different fashions next to each other. b) A large area TEM image of the LC-coated GNRs displaying a micrometer scale assembly; inset shows the typical gold electron diffraction pattern (small selected spot size for selected area electron diffraction).

remarkable superlattice of nanorods is shown in Figure 4b. The inset shows the electron diffraction pattern recorded from a part of this area. The observed ring pattern indicates that the entire self-assembly is composed of local ordered domains. Each domain has a superlattice structure with no in-plane orientational correlation among the domains, similar to a non-aligned nematic or smectic liquid crystalline phase. The various, local concentration-dependent packing type also prevented a clear assignment of the ordering of the GNRs in SAXS experiments, because different types of smectic- and nematic-like ordering coexist as shown in Figure 4.

The distances between the GNRs in these assemblies were measured from intensity cross-section profiles of HR-TEM images. One such image is shown in **Figure 5**a. If we assume that the aromatic parts of the LC ligands on the neighboring GNRs overlap, then the distance between the adjacent rods in a side-by-side orientated assembly would correspond to twice the length of the lateral chain connecting the LC ligand to the rod (total length including MPS + side chain of LC), which is ≈4.8 nm, calculated by assuming an all-trans conformation of the hydrocarbon chains in a 3D optimized structure (see Supporting Information, Figure S3). This value matches well with the measured distances between the rods in a staggered arrangement (from TEM), which was determined to be 4.5 ± 0.5 nm (Figure 5a). The colored lines at the top of the figure and in the center indicate the number of rods considered to plot the intensity cross-section profiles. The spacing between the end-to-end eclipsed rods in the middle of the assembly (Figure 5a) is surprisingly very small (≈1.63 nm) compared to those in the staggered conformation, which is initially puzzling. However, the experiments we performed by tilting the TEM grid (≈30°, see Figure 5b,c) clearly indicate that these eclipsed rods still maintain

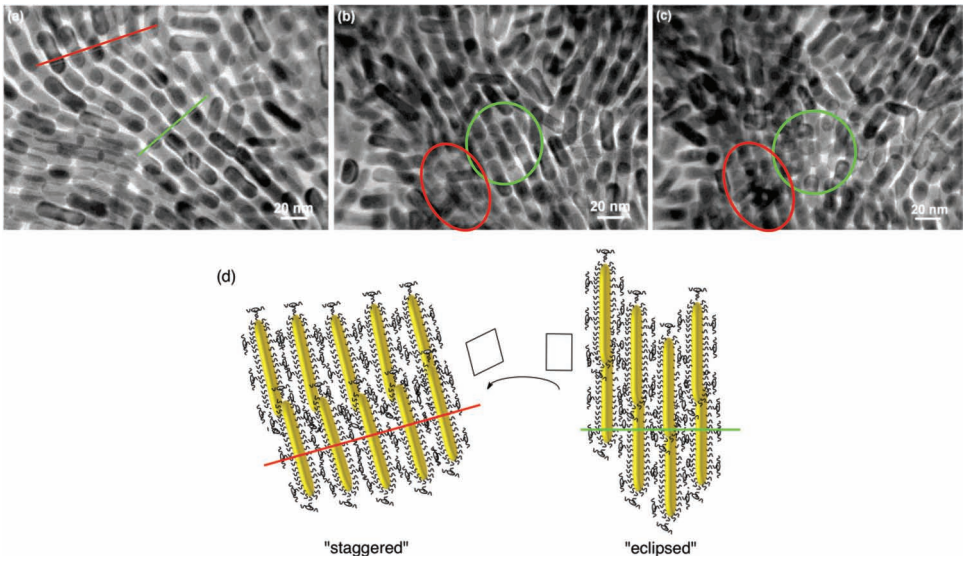

Figure 5. a) HR-TEM image of the GNRs used to measure the distance between the rods in staggered (red line) and eclipsed arrangement (green line). b,c) HR-TEM image of the GNRs at 0°-tilt and at 30°-tilt of the grid, respectively. Scale bars in all three images: 20 nm. On carrying out this operation, the top right corner seems to be unaffected. Red circle: staggered arrangement to eclipsed, green circle: vice versa. d) The cartoon, related to the TEM image in (a), illustrates the different projections of the GNR arrays as observed by TEM. TEM tilting experiments as shown in images (b,c) were used to establish the average side-by-side distance between the GNRs of 4.5 ± 0.5 nm.

a distance of around 4.5 nm between themselves, but they are oriented at an angle to the substrate (green circle in Figure 5c). Thus, it is the viewing angle that gives the false implication that the rods are overlapping on each other, while these rods are situated at an angle to the substrate and maintain a regular distance between them supporting the suggested 3D arrangement (for different projection elucidated by tilting experiments see Figure 5d). The same behavior is observed in most of the formed assemblies. These observations support the assumption that the rod-shaped aromatic parts of the LC ligands overlap (π–π interaction as a driving force) thereby bringing the rods together and inducing a high orientational influence on them. This would explain the perfect line-like assemblies (Figure 4a) formed from the end-to-end attached rods (slightly tilted rods). These results strongly suggest that tuning the number of attached LC ligands and hence their density on the rod surface, should allow for inducing true, fluid nematic or smectic phase behavior in the composite, which is one of our future interests.

It is noteworthy to mention here that the TEM of the well-washed sample showed only short-range side-by-side assembled structures (see Supporting Information, Figure S4). These patterns exhibit merely a local order with no in-plane correlation and isotropic behavior over a large extended area. Li and co-workers recently reported similar short-range side-by-side assemblies for perylene thiol-capped GNRs, where π–π stacking was assumed as a packing force.[39] One possible reason for this behavior could be that the density of the LC ligands on the pure functionalized rods (referred to here as "well washed") is not sufficiently high to induce an orienting influence on the rods over large extended areas. On the other hand, once-washed samples with a miniscule amount of the free **LC2** ligand present, exhibit highly ordered patterns as shown above. The unbound LC molecules in the composite are highly compatible with the ligands on the GNR surface (because they are structurally identical). Hence, the two components form a homogenous colloidal mixture. The free, unbound LC molecules fill the available space, act as mediators, and provide the necessary interactions, required stability as well as directional orientation to the composite thereby assisting the formation of highly ordered arrays of nanorods. More images supporting the remarkable self-assembly of these GNRs are provided in the Supporting Information (Figure S5–S11).

To ascertain that the GNR nanostructured assemblies form indeed over larger areas and not just in smaller sections on TEM grids we also performed SAXS experiments on both samples, the GNRs with end-on (terminal, **LC1**) as well as side-on (lateral) affixed nematogens (**LC2**). As shown in **Figure 6**, the azimuthally averaged intensity data derived from the 2D

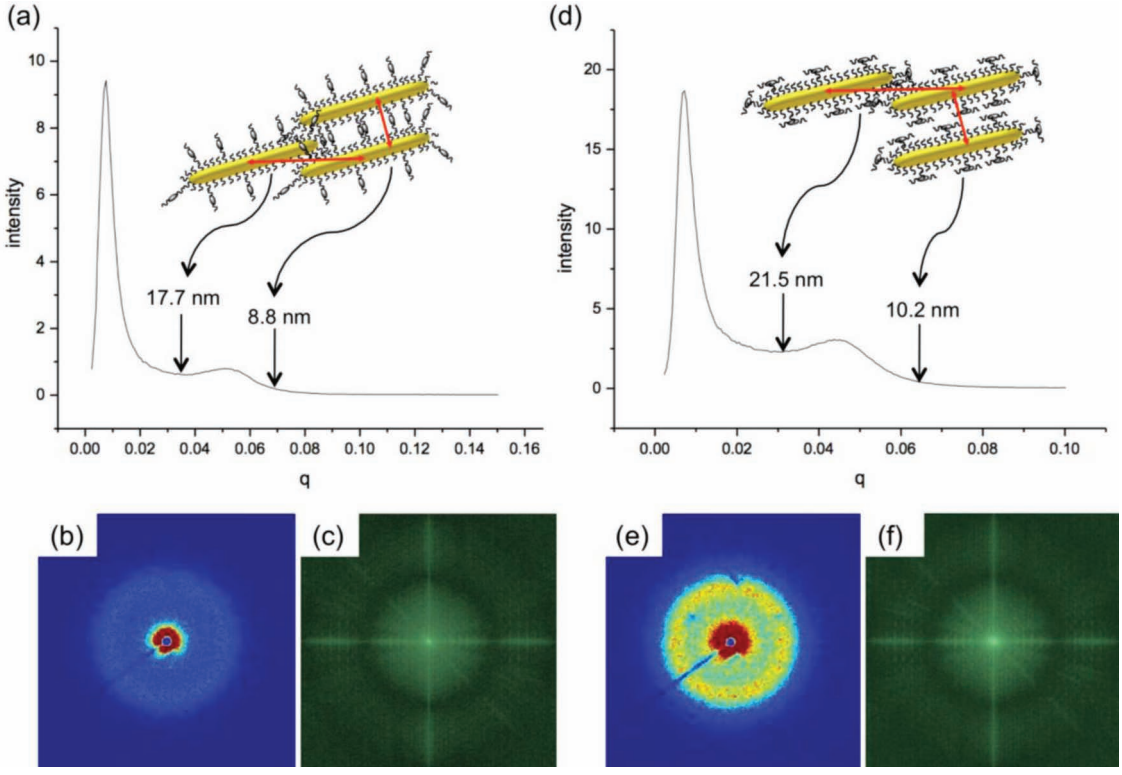

Figure 6. **LC1**-capped GNRs: a) azimuthally averaged intensity data of the scattering vector (q in Å^{-1}) vs. intensity from 2D SAXS pattern shown in (b) and c) Example of a Fourier transform (FFT) obtained from TEM images such as the one shown in Figure 1a. **LC2**-capped GNRs: d) azimuthally averaged intensity data of the scattering vector (q in Å^{-1}) vs. intensity from 2D SAXS pattern shown in (e) and f) example of a Fourier transform (FFT) obtained from TEM images such as the ones shown in Figure 3–5 and Supporting Information Figures S5–S11. Insets in (a) and (d) show cartoons demonstrating typical GNR distances found in the arrays imaged by TEM. Hence, the lateral spacing measured by SAXS (≈10.2 nm) confirms the average side-by-side spacing of 4.5 ± 0.5 nm obtained from TEM images (vide supra) considering the width of the GNRs (6.5 ± 1.5 nm). SAXS samples on Kapton windows were prepared similar to TEM samples on Cu grids. The peak at low q is from scattering around the high flux beam stop.

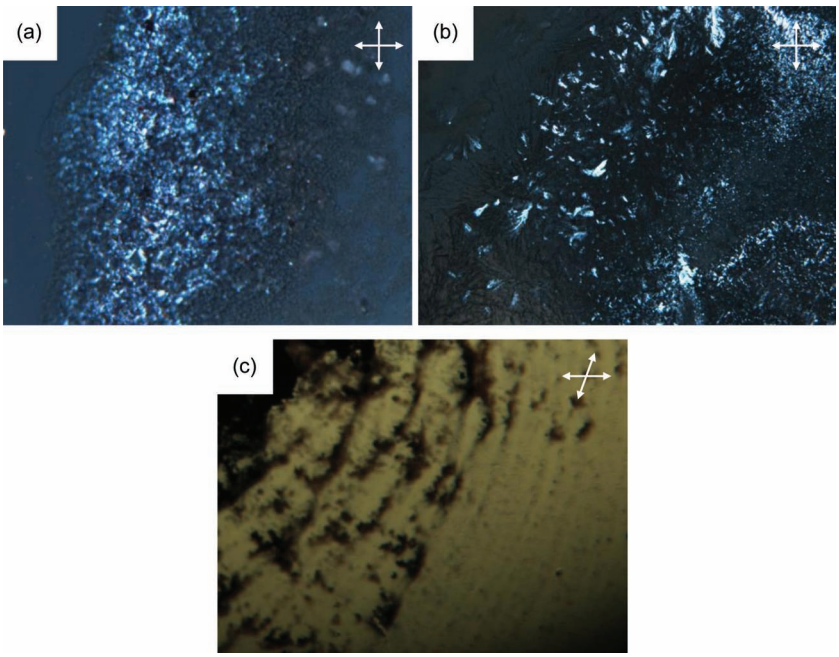

Figure 7. Polarized optical photomicroscopy images of: a,b) the once-washed GNRs on cooling at 75 °C between crossed polarizers (white arrows) and c) the well-washed GNRs on cooling at 80 °C between slightly uncrossed (15°) polarizers.

scattering pattern show only one broad peak corresponding to distances between the **LC1**-capped GNRs from 8.8 nm (side-by-side distance) to 17.7 nm (overlapping longitudinal distance) and for the **LC2**-capped GNRs from 10.2 nm (side-by-side) to 21.5 nm (overlapping longitudinal). These periodicity values are in perfect agreement with the distances measured in the various TEM images and the calculated molecular dimensions of the nematic molecules (with silane conjugation) on the surface of the two GNRs (side-by side for **LC2** and interdigitated for **LC1** as show in the insets of Figure 6a,d). The 2D SAXS patterns also match perfectly with the Fourier transforms (FFT) of the TEM images as shown in Figures 6c,f (shown in the same scale as the 2D SAXS pattern). The different types of GNR arrays detectable in the TEM images, such as different extents of GNR overlap, some more smectic-type arrays, or the few, random isolated rods, most likely cause the lack of two distinct broad scattering maxima in the SAXS pattern one would expect for an unaligned nematic phase with GNRs constituents.

Polarized optical microscopy studies also showed that despite the rather low fraction of free, non-bound nematic LC molecules (only 5 wt% free vs. 95 wt% bound to the GNR surface) in the investigated 'once-washed' GNR composite, birefringent textures are observed between crossed polarizers as shown in **Figure 7**a,b. These textures are non-specific and extremely viscous (to some extent resembling nematic and smectic *Schlieren* textures of high molecular weight or polymeric organic LCs on first heating from an amorphous solid). However, even the well-washed GNR sample with no free, non-bound LC shows birefringence when viewed between crossed polarizers. For the image shown in Figure 7c, the polarizers were slightly uncrossed because of the very high optical density (absorbance) of the sample.

Considering the various methods to assemble GNRs, most are restricted to aqueous medium, produce more confined arrays, and are largely based on electrostatic interactions between the dynamic surfactant molecules on the GNR surface and added external additives.[10–15] In contrast, our approach of covalently functionalizing the nanorods with a suitable liquid crystal molecule (in the presence of a small amount of free LC) offers more dynamically organized patterns which could potentially be further manipulated by external stimuli through LC-mediated reorganizations. Recently we have reported the magnetic field induced orientation of nematic LC end-capped GNRs as discussed earlier (Figure 1a).[31] In the present case, application of a weak magnetic field from a handheld rare earth magnet resulted in the reorientation of the GNR arrays in several areas of the TEM grid as shown in **Figure 8**a–c. This reorientation of the GNRs, achieved at temperatures were the pure **LC2** forms a nematic phase, is here the result of the magnetic field-induced Fréedericksz transition of the **LC2** ligands linked to the GNR surface via silane conjugation assisted by the small quantity of free, non-bound **LC2** molecules in the colloidal mixture (only 1% by weight of the total mixture correspond to non-bound LC molecules). If both, the quantity of free LC molecules is enhanced (by adding an additional quantity of a room temperature nematic mixture; here E7), i.e., promoting attractive interactions between the rods as well as diluting the sample to encourage monolayer formation on the grid, and the magnetic field strength increased to 1.3 T using an electromagnet, reorientation of **LC1**-capped GNRs into hexagonal-ordered arrays extending several hundred nm^2 can be achieved (Figure 8d).

Overall, these initial experiments with the above-described lateral LC-capped GNRs provide intriguing starting points for further exploration regarding the manipulation of the GNR arrays using thermal annealing methods and/or applied magnetic fields. The described observations clearly highlight both feasibility and versatility of LC-guided self-assembly of GNRs with a unique advantage over other methods provided by the on-demand reorientation of arrays using external stimuli. A related example of such GNR reorientation in electric fields was recently disclosed by Richardson and co-workers for short-range ordered hexagonally packed GNR suspended in a nematic liquid crystal (5CB).[40] The key difference in the present work is that the GNRs assemble into nematic and to some degree smectic-type arrays with only a miniscule amount of free liquid crystal molecules (about 1% by weight). Hence, the free liquid crystal acts here as the dopant (or suspended entity promoting attractive interactions between GNRs) in contrast to GNR suspensions investigated by others. Remarkably then, the obtained nematic-type arrays can be magnetically reoriented similar to purely organic nematic liquid crystals. Additional experiments also indicate that it is also possible to extend the self-assembly

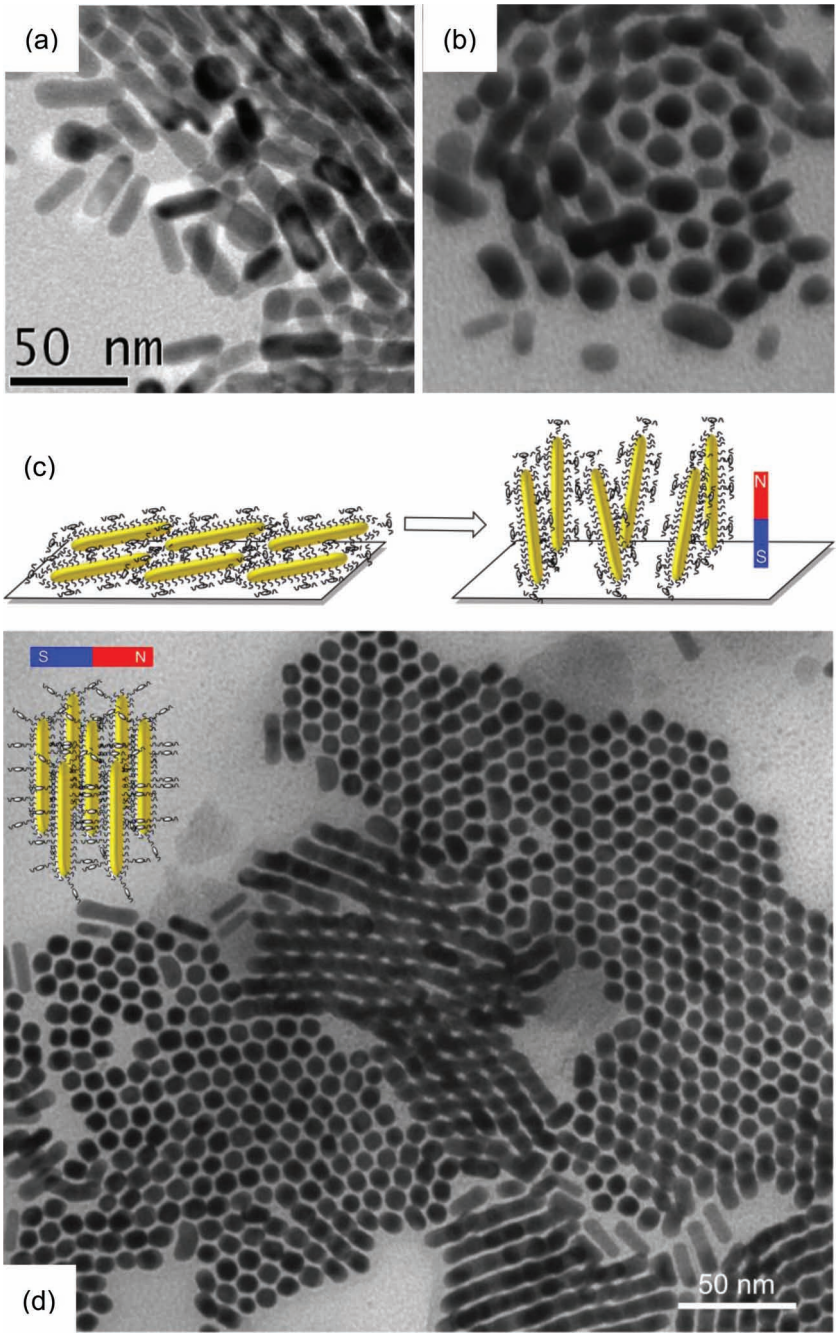

Figure 8. a,b) HR-TEM images of **LC2**-capped GNRs: a) prior to applying a magnetic field and b) after applying a magnetic field (using 1 cm in diameter rare earth disc magnets) at elevated temperature (within the nematic phase range of **LC2**). Scale bar in (a) vis alid for both images. The index grid was removed from the TEM instrument and inserted again after the magnetic field was applied. Care was taken to image almost the same area of the indexed grid. c) Schematic presentation of the magnetic field induced reorientation of the **LC2**-capped GNRs. d) Magnetic field induced assembly and alignment of **LC1**-functionalized GNRs in a 1:1 (by weight) mixture with E7 (using a LakeShore electromagnet at 1.3 T). Hexagonal close-packed assemblies can be seen extending hundreds of nm^2.

behavior of nematic LC-capped GNRs to discotic LC-capped GNRs by covalently functionalizing GNRs with suitable discotic LC moieties forming columnar phases in a similar fashion as described here.[41]

3. Conclusions

In summary, we described an exceptionally effective and versatile method for the self-assembly of GNRs provided by the functionalization with a laterally linked nematogenic LC ligand. These LC-capped GNRs display a rich variety of reproducible self-assembly leading to large-scale ordered superstructures with a variety of morphologies comparable to nematic to smectic LC morphologies on slow evaporation of the solvent on TEM grids. We report for the first time that GNR superstructures once formed can be reorientated simply by placing the sample in a magnetic field. The birefringence observed for these GNRs in thin film between crossed polarizers additionally supports the formation of self-assembled ordered LC-like anisotropic superstructures. Such systems have great significance as future metamaterials, SERS substrates, nanorod-based high efficiency polarizers, and other prominent applications in biological and technological fields.

4. Experimental Section

Synthesis: Compound **1** (0.4 g, 0.5 mmol) was dissolved in dry toluene (10 mL) and trimethoxysilane (0.31 mL, 2.5 mmol) added under nitrogen atmosphere and stirred for 30 min. To this solution, 1,1,3,3-tetramethyldisiloxane Pt-complex (Karstedt's catalyst, 0.1 M) in xylene (50 µL, 0.01 eq.) was added and stirring continued for further 18 h maintaining the nitrogen atmosphere. The solvent and excess trimethoxysilane was removed under vacuum resulting in a light brown residue. Attempts to purify the silane from this residue using column chromatography (both silica and alumina) were unsuccessful, and the mixture contained mainly silane **LC2** and some isomerized **1** (28% as calculated from NMR) with a migrated double bond (vinyl → allyl). Cr 67 (N 86) Iso (monotropic nematic phase observed by POM); ^{1}H NMR (300 MHz, $CDCl_3$, δ ppm): 8.19 (d, 2H, Ar-H), 8.06 (d, 1H, Ar-H), 7.66-7.59 (m, 4H, Ar-H), 7.32-7.25 (m, 4H, Ar-H), 6.98 (d, 2H, Ar-H), 6.58-6.51 (m, 2H, Ar-H), 5.42 (m, 0.62H, -CH=CH-), 4.11-4.01 (m, 6H, -O-CH_2), 3.6 (s, 9H, -Si-$(OCH_3)_3$), 1.92-1.80 (m, -CH_2-CH=CH), 1.41-1.60 (m, 6H, -O-CH_2-CH_2), 1.22 -1.40 (m, 36H, -CH_2-), 1.0-0.82 (m, 9H, -CH_3), 0.68-0.61 (m, 1.44H, -CH_2-Si-$(OCH_3)_3$); IR (KBr): ν_{max} = 2922, 2853, 1739, 1722, 1606, 1569, 1510, 1493, 1467, 1433, 1393, 1254, 1204, 1164, 1135, 1075, 1038, 872, 849, 792, 759, 719, 689, 653 and 507 cm^{-1}.

The percentage of silane in the mixture was estimated using characteristic peaks in the ^{1}H NMR of the residue, i.e. by comparing the ratio of the integration of the methyl peak at 0.65 ppm [(-**CH_2**-Si-$(OCH_3)_3$) due to compound **LC2**] to the alkene proton peak at 5.42 ppm [(-CH=CH-) due to the migrated double bond in compound **1**], which provided a yield of 72% for the reaction described above. Based on the estimated

percentage yield of silane from the NMR, the residue was dissolved in chloroform to make a 10 mM solution, where only the silane will react in the subsequent condensation step.

The coating exchange of CTAB on the GNR surface with nematic ligands was carried out as described below. A measured volume (3 mL) of CTAB-capped GNRs was washed once with an equal volume of chloroform in order to remove the excess free ligand. The washed rods were treated with an appropriate volume (120 µL) of MPS (10 mM solution in ethanol) and vortexed for 2–3 min. The resulting colloidal solution was allowed to stand at room temperature for 30 min. Thereafter, the nematic silane solution (3 mL, 10 mM in chloroform) was added, followed by a base (30 µL, 1 M NaOH), and vortexed again for 2–3 min. Very soon, the change in the color of the solvent clearly indicated the coating exchange of CTAB GNRs with nematic LC and their subsequent phase transfer from the water to the organic chloroform phase. Upon exchange, the water phase becomes clear and the chloroform phase becomes dark brown in color as shown in Figure S1 (Supporting Information). The organic phase was separated and stirred at room temperature overnight to ensure the completeness of the capping process. The resulting solution was ultracentrifuged (16 000 rpm, 20 min) to remove the excess free ligand. The nanorod precipitate was redispersed in toluene and centrifuged again. The process of precipitation and redispersion were repeated several times until the last supernatant was free from any residual non-bound silane/siloxane as confirmed by ^{1}H NMR. This excess ligand-free sample was used for UV-vis-NIR and FTIR measurements shown in Figure 2. However, our investigations demonstrated that the once centrifuged sample with a small amount of free LC ligand (≈150 µL of 10 mM free LC in a 1 mL GNR dispersion, 5 wt% free vs. 95 wt% bound to the GNR surface) present produces exceptional self-assembled superstructures of GNRs compared to the well-washed sample (no free LC).

Supporting Information

Supporting Information is available from the Wiley Online Library or from the author.

Acknowledgements

The authors would like to thank the Province of Manitoba for a grant from the Science and Technology International Collaboration Fund, the Natural Science and Engineering Research Council (NSERC) of Canada, the Canada Foundation for Innovation (CFI), and the Manitoba Research and Innovation Fund (MRIF) for financial support. T.H. also acknowledges financial support from Kent State University and the Government of Ohio's Third Frontier Program for Ohio Research Scholars. Special thanks go to Dr. Kevin McEleney for his help with the SAXS measurements and to Andre Dufresne for all the help and assistance with TEM imaging.

Received: July 31, 2012
Revised: September 17, 2012
Published online: October 16, 2012

[1] S. Link, M. A. El-Sayed, *Annu. Rev. Phys. Chem.* **2003**, *54*, 331.
[2] M. E. Stewart, C. R. Anderton, L. B. Thompson, J. Maria, S. K. Gray, J. A. Rogers, R. G. Nuzzo, *Chem. Soc. Rev.* **2008**, *108*, 494.
[3] P. K. Jain, X. H. Huang, I. H. El-Sayed, M. A. El-Sayed, *Acc. Chem. Res.* **2008**, *41*, 1578.
[4] M. R. Jones, K. D. Osberg, R. J. Macfarlane, M. R. Langille, C. A. Mirkin, *Chem. Rev.* **2011**, *111*, 3736.
[5] L. Xu, H. Kuang, L. Wang, C. Xu, *J. Mater. Chem.* **2011**, *21*, 16759.
[6] K. Liu, N. Zhao, E. Kumacheva, *Chem. Soc. Rev.* **2011**, *40*, 656.
[7] P. R. Sajanlal, T. S. Sreeprasad, A. K. Samal, T. Pradeep, *Nanoreviews* **2011**, *2*, 5883.
[8] a) X. Huang, I. H. El-Sayed, W. Qian, M. A. El-Sayed, *J. Am. Chem. Soc.* **2006**, *128*, 2115; b) D. Pissuwan, S. M. Valenzuela, C. M. Miller, M. B. Cortie, *Nano Lett.* **2007**, *7*, 3808; c) H. Ding, K. T. Yong, I. Roy, H. E. Padavar, W. C. Law, E. J. Bergey, P. N. Prasad, *J. Phys. Chem. C* **2007**, *111*, 12552.
[9] a) L. R. Hirsch, R. J. Stafford, J. A. Bankson, S. R. Sershen, B. Rivera, R. E. Price, J. D. Hazle, N. J. Halas, J. L. West, *Proc. Natl. Acad. Sci. USA* **2003**, *100*, 13549; b) L. Tong, Y. Zhao, T. B. Huff, M. N. Hansen, A. Wei, J. X. Chen, *Adv. Mater.* **2007**, *19*, 3136; c) R. S. Norman, J. W. Stone, A. Cole, C. J. Murphy, T. L. Sabo-Attwood, *Nano Lett.* **2008**, *8*, 302; d) W. Zhang, J. Meng, Y. Ji, X. Li, H. Kong, X. Wu, H. Xu, *Nanoscale* **2011**, *3*, 3923; e) K. Y Lin, A. F. Bagley, A. Y. Zhang, D. L. Karl, S. S. Yoon, S. N. Bhatia, *Nano Life* **2010**, *1*, 277.
[10] a) N. R. Jana, T. Pal, *Adv. Mater.* **2007**, *19*, 1761; b) K. D. Alexander, K. Skinner, S. P. Zhang, H. Wei, R. Lopez, *Nano Lett.* **2010**, *10*, 4488; c) L. Zhong, X. Zhou, S. Bao, Y. Shi, Y. Wang, S. Hong, Y. Huang, X. Wang, Z. Xie, Q. Zhang, *J. Mater. Chem.* **2011**, *21*, 14448.
[11] B. Nikoobakht, Z. L. Wang, M. A. El-Sayed, *J. Phys. Chem. B* **2000**, *104*, 8635.
[12] F. Kim, S. Kwan, J. Akana, P. Yang, *J. Am. Chem. Soc.* **2001**, *123*, 4360.
[13] T. Sau, C. J. Murphy, *Langmuir* **2005**, *21*, 2923.
[14] a) T. S. Sreeprasad, A. K. Samal, T. Pradeep, *Langmuir* **2008**, *24*, 4589; b) T. S. Sreeprasad, T. Pradeep, *Langmuir* **2011**, *27*, 3381.
[15] K. Mitamura, T. Imae, N. Saito, O. Takai, *J. Phys. Chem. B* **2007**, *111*, 8891.
[16] a) E. Dujardin, L. Hsin, C. R. Chris Wang, S. Mann, *Chem. Commun.* **2001**, 1264; b) B. Pan, D. Cui, C. Ozkan, P. Xu, T. Huang, Q. Li, H. Chen, F. Liu, F. Gao, R. He, *J. Phys. Chem. C* **2007**, *111*, 12572.
[17] C. Hamon, M. Postic, E. Mazari, T. Bizien, C. Dupuis, P. Even-Hernandez, A. Jimenez, L. Courbin, C. Gosse, F. Artzner, V. Marchi-Artzner, *ACS Nano* **2012**, *6*, 4137.
[18] N. Kanayama, O. Tsutsumi, A. Kanazawa, T. Ikeda, *Chem. Commun.* **2001**, 2640.
[19] I. In, Y. Jun, Y. J. Kim, S. Y. Kim, *Chem. Commun.* **2005**, 2640.
[20] L. Cseh, G. H. Mehl, *J. Am. Chem. Soc.* **2006**, *128*, 13376.
[21] V. A. Mallia, P. K. Vemula, G. John, A. Kumar, P. M. Ajayan, *Angew. Chem. Int. Ed.* **2007**, *46*, 3269.
[22] X. Zeng, F. Liu, A. G. Fowler, G. Ungar, L. Cseh, G. H. Mehl, J. E. Macdonald, *Adv. Mater.* **2009**, *21*, 1746.
[23] H. Qi, B. Kinkead, V. M. Marx, H. R. Zhang, T. Hegmann, *ChemPhysChem* **2009**, *10*, 1211.
[24] M. Wojcik, W. Lewandowski, J. Matraszek, J. Mieczkowski, J. Borysiuk, D. Pociecha, E. Gorecka, *Angew. Chem. Int. Ed.* **2009**, *48*, 5167.
[25] M. Draper, I. M. Saez, S. J. Cowling, P. Gai, B. Heinrich, B. Donnio, D. Guillon, J. W. Goodby, *Adv. Funct. Mater.* **2011**, *21*, 1260.
[26] M. Yamada, Z. Shen, M. Miyake, *Chem. Commun.* **2006**, 2569.
[27] S. Kumar, S. K. Pal, P. S. Kumar, V. Lakshminarayanan, *Soft Matter* **2007**, *3*, 896.
[28] V. M. Marx, H. Girgis, P. A. Heiney, T. Hegmann, *J. Mater. Chem.* **2008**, *18*, 2983.
[29] H. Park, A. Agarwal, N. A. Kotov, O. D. Lavrentovich, *Langmuir* **2008**, *24*, 13833.
[30] Q. Liu, Y. Cui, D. Gardner, X. Li, S. He, I. I. Smalyukh, *Nano Lett.* **2010**, *10*, 1347.
[31] S. Umadevi, X. Feng, T. Hegmann, *Ferroelectrics* **2012**, *431*, 164.

[32] S. Diez, D. A. Dunmur, M. R. De la Fuente, P. K. Karahaliou, G. H. Mehl, T. Meyer, M. A. P. Jubindo, D. J. Photinos, *Liq. Cryst.* **2003**, *30*, 1021.
[33] D. Apreutesei, G. H. Mehl, *Chem. Commun.* **2006**, 609.
[34] N. R. Jana, *Small* **2005**, *1*, 875.
[35] a) S. Link, M. A. El-Sayed, *J. Phys. Chem. B* **1999**, *103*, 8410; b) Y. Yu, S. Chang, C. Lee, C. R. C. Wang, *J. Phys. Chem. B* **1997**, *101*, 6661; c) S. Link, M. B. Mohamed, M. A. El-Sayed, *J. Phys. Chem. B* **1999**, *103*, 3073; d) M. M. Miller, A. A. Lazarides, *J. Phys. Chem. B* **2005**, *109*, 21556; e) H. Wang, D. W. Brandl, F. Le, P. Nordlander, N. J. Halas, *Nano Lett.* **2006**, *6*, 827; f) T. K. Sau, A. L. Rogach, F. Jäckel, T. A. Klar, J. Feldmann, *Adv. Mater.* **2010**, *22*, 1805.
[36] For examples, see: a) J. J. Mock, D. R. Smith, S. Schultz, *Nano Lett.* **2003**, *3*, 485; b) C. Yu, L. Varghese, J. Irudayaraj, *Langmuir* **2007**, *23*, 9114; c) A. Wijaya, K. Hamad-Schifferli, *Langmuir* **2008**, *24*, 9966; d) Z. R. Guo, C. R. Gu, X. Fan, Z. P. Bian, H. F. Wu, D. Yang, N. Gu, J. N. Zhang, *Nanoscale Res. Lett.* **2009**, *4*, 1428.
[37] a) H. Jiang, Z. Zheng, Z. Li, X. Wang, *Ind. Eng. Chem. Res.* **2006**, *45*, 8617; b) H. K. Park, T. H. Ha, K. Kim, *Langmuir* **2004**, *20*, 4851; c) D. Blaudez, M. Bonnier, B. Desbat, F. Rondelez, *Langmuir* **2002**, *18*, 9158.
[38] E. Rabani, D. R. Reichman, P. L. Geissier, L. E. Brus, *Nature* **2003**, *426*, 271.
[39] C. Xue, Q. Birel, M. Gao, S. Zhang, L. Dai, A. Urbas, Q. Li, *J. Phys. Chem. C* **2012**, *116*, 10396.
[40] M. R. Thomas, S. Klein, R. J. Greasty, S. Mann, A. W. Perriman, R. M. Richardson, *Adv. Mater.* **2012**, *24*, 4424.
[41] GNR packing facilitated by π–π stacking: X. Feng, S. Umadevi, T. Hegmann, unpublished.